# A study of the near-infrared modulation at spin and orbital periods in the intermediate polar WX Pyx

V. H. Joshi*, N. M. Ashok and D. P. K. Banerjee

*Physical Research Laboratory, Ahmedabad 380 009, India*

**Abstract.** We present near-infrared *J*-band photometric observations of the intermediate polar WX Pyx. The frequency analysis indicates the presence of a period at 1559.2±0.2 sec which is attributed to the spin period of the white dwarf. The spin period inferred from the infrared data closely matches that determined from X-ray and optical observations. WX Pyx is a system whose orbital period has not been measured directly and which is not too well constrained. From the IR observations, a likely peak at 5.30±0.02 hr is seen in the power spectrum of the object. It is suggested that this corresponds to the orbital period of the system. In case this is indeed the true orbital period, some of the system physical parameters may be estimated. Our analysis indicates that the secondary star is of M2 spectral type and the distance to the object is 1.53 kpc. An upper limit of 30° for the angle of inclination of the system is suggested. The mass transfer rate and the magnetic moment of the white dwarf are estimated to be $(0.95-1.6)\times10^{-9} M_\odot$ yr$^{-1}$ and $(1.9-2.4)\times10^{33}$ G cm$^3$ respectively.

## 1. Introduction

Intermediate polars (IPs) are a sub-class of magnetic cataclysmic variable stars (mCVs). An IP comprises of a semi-detached binary system consisting of a white dwarf primary star and a late-type Roche-lobe filled secondary star; the white dwarf is believed to have a moderate magnetic field strength of B~1−10 MG (Patterson 1994). The rotation period of the white dwarf is not synchronized with the binary orbital period. The mass transferred from the secondary to the primary, by the process of Roche lobe overflow, eventually accretes onto or near the magnetic poles of the white dwarf through the magnetic field lines. The shock heated plasma produces

---

*email: vjoshi@prl.res.in

X-rays by the cooling of electrons near the white dwarf's surface through free-free interactions (Evans & Hellier 2007). Recently, Bednarek & Pabich (2010) have proposed that $\gamma$ rays could also be produced when the accelerated hadrons are convected to the white dwarf surface and interact with the dense matter. A comprehensive review of IPs may be found in Warner (1995).

WX Pyx was identified as 1E 0830.9-2238 in the Galactic plane survey of Einstein X-ray observatory by Hertz & Grindlay (1984). The blue excess seen in the object and also the nature of the optical spectra, which displayed emission lines including Hydrogen Balmer lines, HeI and HeII - lines which are typically seen in the spectra of CVs - suggested the object as a CV candidate (Hertz et al. 1990). The strong presence of the high-excitation HeII 4686 Å line in the optical spectrum also suggested the possibility of a magnetic nature for the system (Hertz et al. 1990). From an analysis of the optical light curve O'Donoghue (1996) found a stable period of ~26 min which was attributed to the spin period of the white dwarf and confirmed the IP nature of the WX Pyx system. They suggested a value of of ~6 to 9 hr for the orbital period, based on spectroscopic and photometric data, but stressed that this result was not robust and should be viewed with caution. Though there are no direct X-ray observations of WX Pyx available till date, the object was accidentally detected 10.5 arcmin off-axis during a pointed observation of NGC 2613 by XMM-Newton. Schlegel (2005) analyzed data related to this serendipitous X-ray detection and found a spin period of 1557.3 s which matched well with the optical spin-period estimate of O'Donoghue (1996). An orbital period of ~5.54 hr was inferred indirectly from the separation of spin-orbital side band frequencies in the power spectrum.

The present study is partially motivated by the fact that there are no infrared studies of WX Pyx. More importantly, we had hoped to determine more robustly the orbital period of the system for which no direct observational evidence is available. Such a determination would allow many of the system parameters and mode of accretion of WX Pyx to be better estimated. In this study we present photometric observations at near-IR $J$ band and undertake a time series analysis to estimate the orbital and spin period of the object.

## 2.    Observations and data analysis

Near infrared $J$ band photometry of WX Pyx was done using the Mt.Abu 1.2-m telescope. The object was observed for a total duration of 22 hr spanning six nights from December 2007 to February 2010. The observations were taken using the Near-Infrared Imager/Spectrometer which uses a 256×256 HgCdTe NICMOS3 array with a FOV of 2×2 arcmin$^2$. The telescope was dithered at 5 different positions during observations, as is customary for IR observations (for e.g. Das et al. 2008), to produce median sky-cum-dark frames for individual images. Several selected field stars were always kept in the field of view while dithering to enable differential photometry to be done. Frames of smaller durations were co-added when single frames of larger duration were not available. Flat fielding, using twilight flats, was done to ensure a proper pixel response of the detector. An appropriate median sky-cum-dark image was generated and subtracted from the object frames. Instrumental magnitudes, obtained from these sky-subtracted

**Table 1.** Log of the photometric observations.

| Date of observations (dd/mm/yyyy) | Reduced JD | Filter | Exp. time (sec) | Time cover- age (hr) | Spin cycles covered |
|---|---|---|---|---|---|
| 18/12/2007 | 54452 | J | 180 | 4.5 | 10 |
| 19/12/2007 | 54453 | J | 180 | 3.9 | 9 |
| 18/01/2008 | 54483 | J | 60 | 3.3 | 7.5 |
| 18/03/2009 | 54909 | J | 60 | 4.1 | 9.5 |
| 19/03/2009 | 54910 | J | 60 | 4.0 | 9.5 |
| 22/02/2010 | 55250 | J | 180 | 2.2 | 5 |

Note: Reduced JD = JD - 2400000

frames using aperture photometry, were finally flux calibrated by comparing with several field stars whose lightcurves had previously been checked for photometric stability.

The routines used for data reduction are based on the Interactive Data Language (IDL) package. Specifically, APER procedure from GSFC IDL astronomy user's library was used for synthetic aperture photometry. The log of the observations is given in Table 1, which gives the date of observations, filter information, exposure time, total observation coverage and the number of spin cycles covered. The *J*-band photometric data are listed in the Appendix.

## 3.   Results and discussion

### 3.1   Light curves and frequency analysis

The light curves of individual nights are shown in Fig. 1 along with their corresponding periodograms. A clear modulation at a period close to 26 min can be visually seen in all the light curves. Equivalently, analysis yields the presence of strong peak near 0.64 mHz in all the periodograms. The mean *J* magnitude of the program star, peak frequency and semi-amplitude of the light curve on individual nights are presented in Table 2. The peak frequency varies between 0.6367 mHz to 0.6439 mHz in periodograms of individual runs. This variation of 0.007 mHz, however, is much below the error level estimated from half width at half maximum of the peak which is 0.02 mHz.

Rapid but weak oscillations at frequencies other than that of the principal component at 0.64 mHz were also observed in certain light curves. Notable among these is the one near 1.2 mHz which is the first harmonic of the spin period. In order to check the coherence of these weak oscillations we plotted the periodograms up to the Nyquist frequency for all the light curves of individual nights. We do not find any coherent frequency above 0.64 mHz. We thus conclude that these weak oscillations may be due to flickering in the light curve, a feature which is a common characteristic of CVs.

**Table 2.** Frequency analysis of daily lightcurves.

| Reduced JD of observation | Mean J magnitude | Peak frequency (mHz) | Semi-amplitude (mag) |
|---|---|---|---|
| 54452 | 15.54 | 0.6367 | 0.14 |
| 54453 | 15.51 | 0.6372 | 0.16 |
| 54483 | 15.53 | 0.6413 | 0.11 |
| 54909 | 15.57 | 0.6439 | 0.12 |
| 54910 | 15.51 | 0.6418 | 0.12 |
| 55250 | 15.56 | 0.6421 | 0.11 |
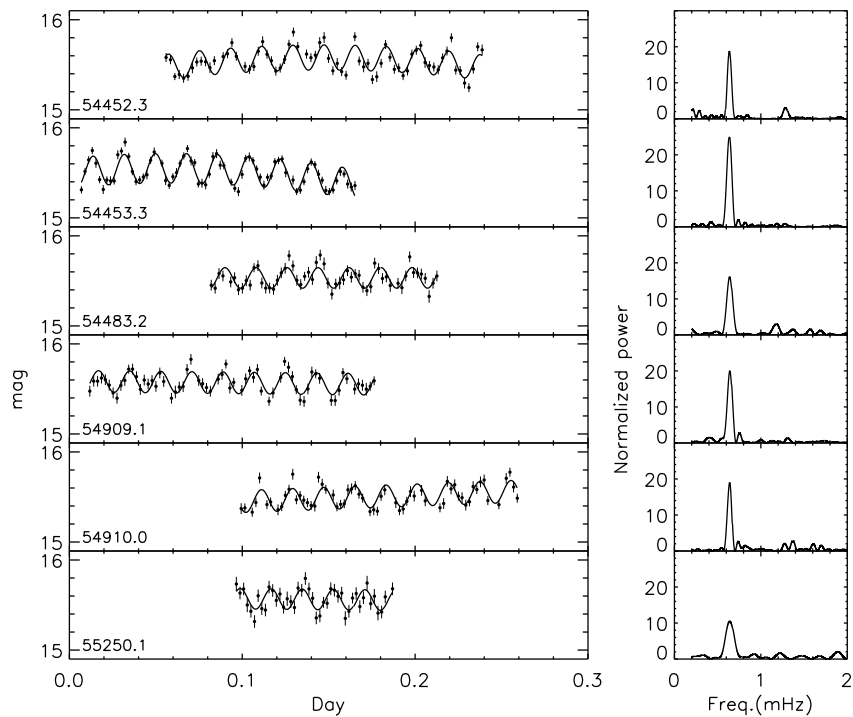


**Figure 1.** Light curves of all the nights listed in Table 1 are shown in the panels on the left. The abscissa is HJD - HJD0 where HJD0 is arbitrary and given in the lower left for each day. Solid line shows the best fit sinusoid plus a polynomial fit representing the long term variation. The Lomb-Scargle periodograms of individual runs are shown in the right hand panels. It may be noted that the periodograms extend up to the Nyquist frequency.
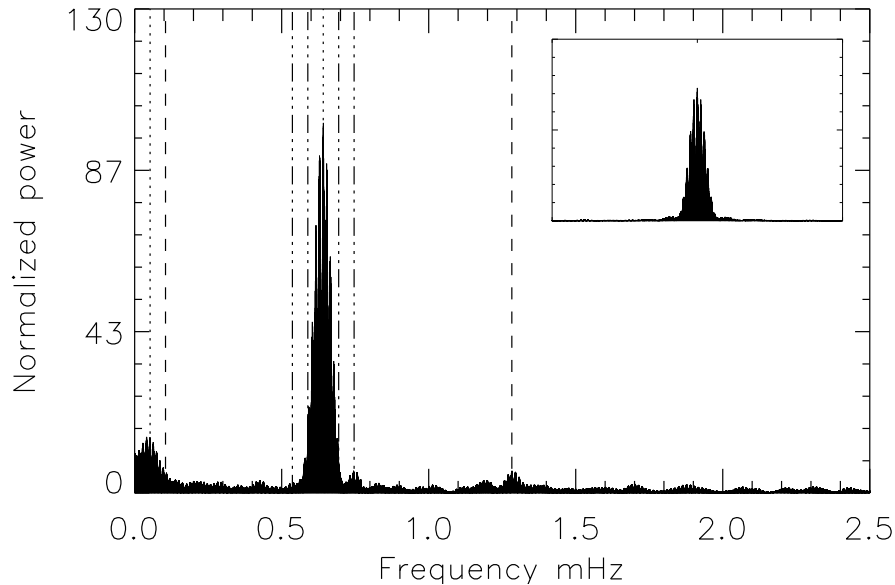
**Figure 2.** The Lomb-Scargle periodogram of all the data is shown. The dotted lines indicate orbital and spin frequencies. The dashed lines show the first harmonic of the orbital and spin periods whereas the dot-dashed lines represents the spin-orbital sidebands. The window function is plotted as an inset in the top of the figure.

The periodogram of the combined data plotted till the Nyquist frequency is shown in Fig. 2. A strong peak can be seen near 0.64 mHz. Another noteworthy peak is at the low frequency end of the periodogram near 50 $\mu$Hz which is discussed subsequently. One can also see minor peaks corresponding to 0.74 mHz and 1.28 mHz. But we consider these latter peaks to be statistically insignificant because the associated power is at a level of only 2 sigma above the background. Temporal gaps of various lengths in the observed data set cause the various aliasing peaks to be present in the periodogram of Fig. 2. One day aliases are dominant in particular. This can be clearly seen in a plot of the window function which is presented as an inset in Fig. 2. The periodogram between frequencies 0.4 and 0.9 mHz is shown in Fig. 3 which is magnified part of the region containing peak near 0.64 mHz frequency. The highest power is at a frequency of 0.64134±0.00008 mHz which corresponds to a period of 1559.2±0.2 sec. It may be noted that the formal error of the frequency (or period) is estimated by half-width at half-maximum of the highest peak in the peridogram which is the conventional way to determine the error.

It is possible to generate the pulse profile of the spin modulation from the entire data set. As a first step, a best fit polynomial of either degree one or two was subtracted from data of individual nights to remove the long-term variation from the light curve. The data were then folded at a period 1559.2 sec. The phase was divided into 25 bins to produce the spin pulse profile which is presented in Fig. 4. The error in each bin is inferred from the standard deviation of the data
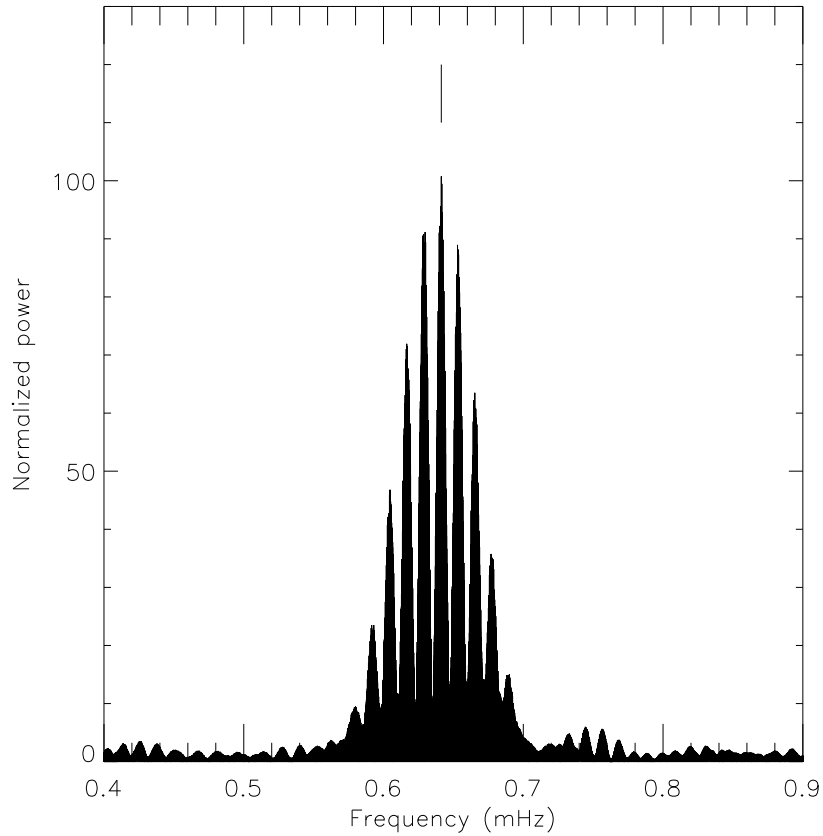
**Figure 3.** The LS periodogram of all the data near the spin frequency, which is marked with a vertical dash at 0.64134 mHz, is shown.

points within the bin. From our analysis we find that the time of maximum of the oscillation is at RJD 54322.03408±0.00005 d.

In Fig. 2, another significant peak is seen at a much lower frequency near 50 $\mu$Hz. A Lomb-Scargle periodogram produced around this frequency, in the range 0.02 $\mu$Hz to 200 $\mu$Hz, is shown in Fig. 5. In this periodogram the maximum power is present at a frequency of 52.43075 $\mu$Hz corresponding to a period of ~5.3 hr. However, various alias peaks are strong in this spectrum and the 1-day alias in particular, at a frequency of 40.45529 $\mu$Hz or alternatively corresponding to a period of ~6.9 hr, is of comparable power to the 5.3 hr peak. It is thus possible that either one of these periods (i.e 5.3 or 6.9 hr) may correspond to the orbital period but it is difficult to discriminate between the two based solely on our data.
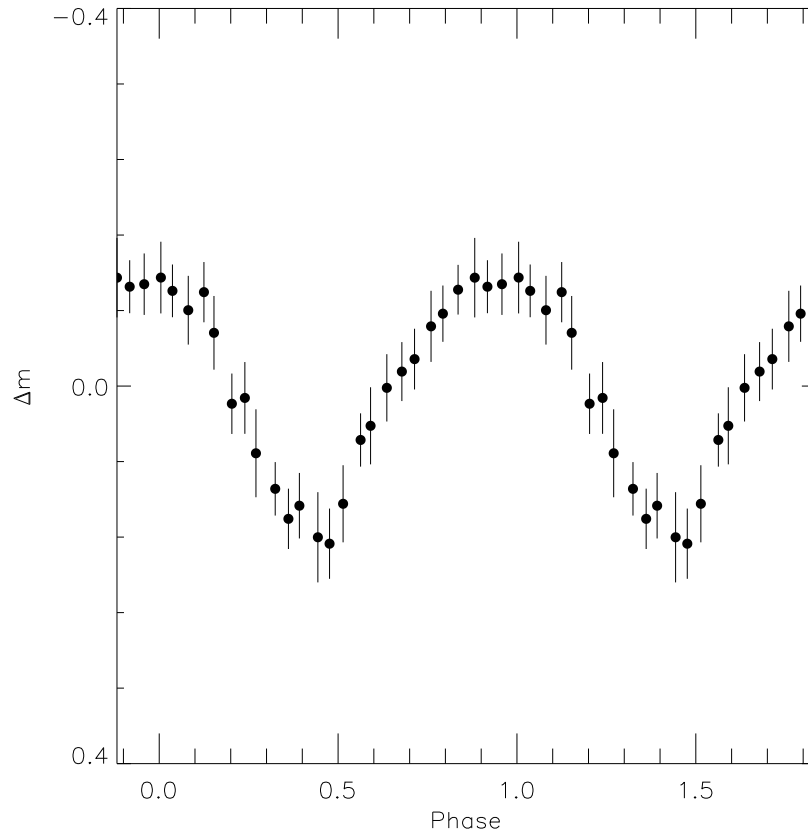
**Figure 4.** The binned pulse profile folded at 1559.2 sec corresponding to the white dwarf spin period. The complete cycle is divided into 25 bins. The ordinate represents the relative magnitude and the abscissa represents the fractional phase. The spin cycle is repeated once for clarity.

However, we propose that the 5.3 h period more likely corresponds to the orbital period of the binary system. First, the period of 5.3 hr is in reasonably good agreement with the orbital period of 5.54 h inferred by Schlegel (2005) from the separation of spin-orbit sideband peaks in the power spectrum of the X-ray data. Moreover a peak-like feature, albeit of weak power, is seen at a frequency 0.74478 mHz in Fig. 2. If the 5.3 h period is correct, then such a feature is expected to arise as a result of the $\omega + 2\Omega$ sideband peak. On the other hand, if the 6.9h period is correct, then based on the same argument advanced above, we should expect a feature at 0.73240 mHz which is however not seen. In summary, there are indications from our data for a 5.3 h orbital period in the WX Pyx system. The evidence for this is not overwhelming, but when results from the X-ray data are also considered collectively, the 5.3 h period appears to be a realistic possibility.
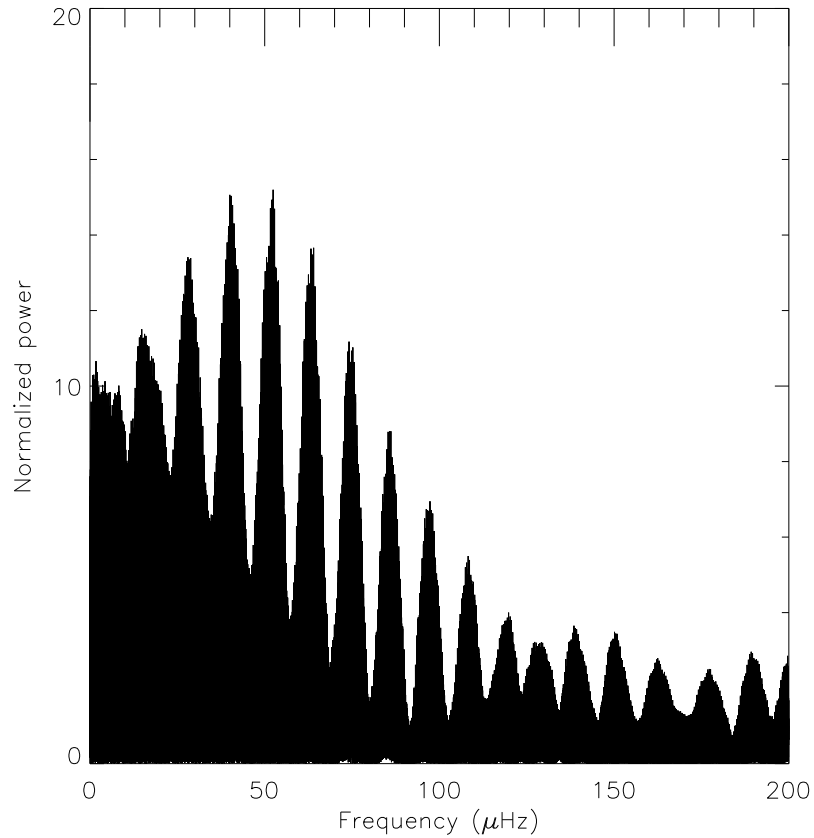
**Figure 5.** The LS periodogram near the orbital frequency is shown. It may be noted that there is no significant power above the noise level at the first harmonic of the orbital frequency.

We thus assume that 5.30±0.02 hr as the orbital period and adopt it, in following subsections, to determine some of the system parameters of WX Pyx. The orbital phase plot of WX Pyx is given in Fig. 6 using a precise value of 5.297 hr (19072 sec) for the orbital period. The time of the maximum light of the orbital modulation is found to be RJD 54327.1897±0.0002 d.

## 3.2 Spectral type of the secondary

It is well established that the secondary star in cataclysmic variables, with period less than 6 hr, resemble late-type main sequence stars i.e. stars of spectral type K or M. However, the secondary stars of CVs have been shown to be a little cooler than the isolated main sequence star of same
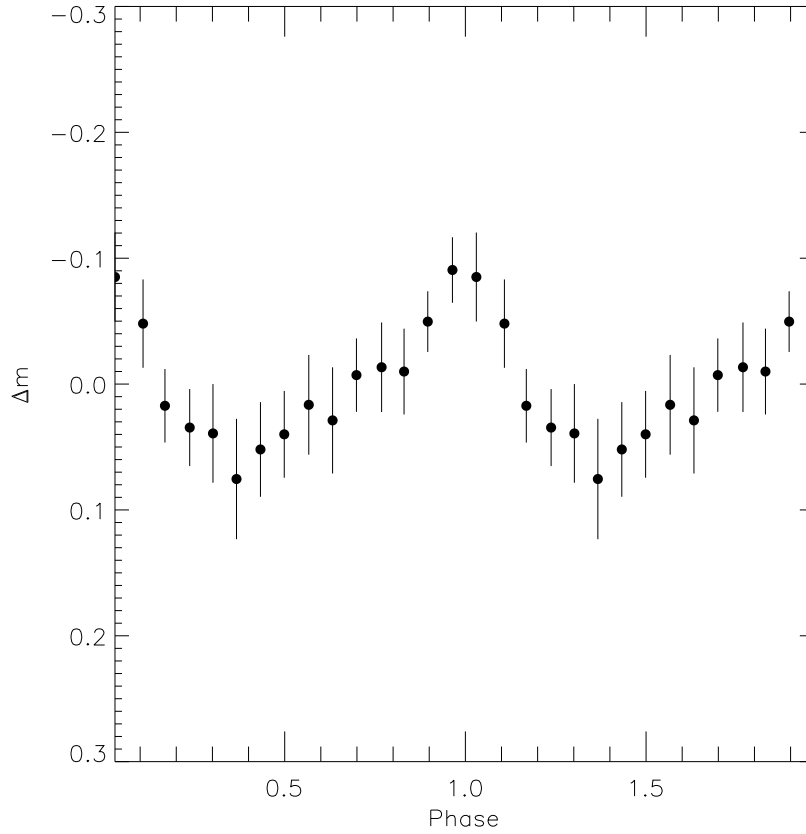
**Figure 6.** The binned phase plot of 5.30 hr corresponding to the orbital period of WX Pyx is shown. The complete cycle is divided into 15 bins. The ordinate represents relative magnitude and the abscissa represents the fractional phase. The profile is repeated once for clarity.

mass and radius (Knigge 2006, and Fig. 7 therein; hereafter K2006). An empirical relationship between orbital period and spectral type has been obtained (Beuermann 1998; K2006). Using the empirical relation discussed in K2006, and assuming an orbital period of 5.3 hr, we estimate the spectral type of the secondary to be constrained in the range M2±2.

### 3.3  Distance to the source

Since the spectral type of the system is known, one can estimate the distance to it using the method first suggested by Bailey (1981). This inter-relates the surface brightness $F_\lambda$ at wavelength $\lambda$, radius of the star $R$, distance $d$ and observed flux $f_\lambda$, by the following relation

$$F_\lambda = f_\lambda \left(\frac{d}{R}\right)^2 \tag{1}$$

Assuming that the late type secondary star is the dominating contributor to the $K$ band flux and expressing flux in magnitudes we can write,

$$S_k = m_K + 5 - 5 log d + 5 log \left(\frac{R}{R_\odot}\right) \tag{2}$$

where $m_K$ is the apparent magnitude and $S_k$ is the surface brightness in the $K$ band . The radius $R$ of the star can be calculated from the Roche-lobe geometry. However, the above approach gives only a lower limit of the distance instead of distance itself because of our assumption that the secondary star is the sole contributor to the $K$ band flux. K2006 discussed the relations between mass-radius and spectral type-orbital period and used these in the above equation to derive the simpler form given below viz.

$$5 log(d_{lim}) = m_K - M_K(P_{orb}) + 5 \tag{3}$$

where $d_{lim}$ is the lower limit to the distance, $m_K$ is observed $K$ band magnitude and $M_K$ is the absolute magnitude as a function of orbital period.

From K2006 we obtain an absolute $K$ band magnitude $M_K = 5.15$ for a 5.3 hr orbital period. The $K_s$ band magnitude of WX Pyx from 2MASS data ($K_s$ mag. = 14.817) was converted to the CIT system using the transformation given by Carpenter (2001) resulting in a transformed CIT $K$ magnitude of 14.857. The use of this value in the last equation gives a lower limit to the distance as 874 pc. However, as pointed out by K2006, the assumption that the secondary contributes predominantly to the $K$ band flux is not necessarily true in a general sense. K2006 studied the objects with well-determined distances based on the parallax method and gave an offset value in magnitudes which is to be applied to estimate better the distance to the object. Applying this offset of 1.22 magnitude for the $K$ band we infer the distance to the source to be $\sim$1.53 kpc.

### 3.4 Mode of accretion onto the white dwarf

In their first optical follow-up observations, Hertz et al. (1990) analyzed the optical spectrum of WX Pyx and calculated the equivalent width of the H$\beta$ emission line. From this, they estimated the *V* band absolute magnitude of the disc $M_v$ using the relation given by Patterson (1984) which correlates these two parameters . They compared $M_v$ with the observed *V* band magnitude to infer that the distance to WX Pyx is ~1.6 kpc. We keep in mind that the relation given by Patterson (1984) holds for IPs with well-developed discs around the white dwarf. Interestingly the distance estimate in this work of ~1.53 kpc, calculated using a different approach, closely matches that of Hertz et al. (1990). The agreement/consistency of two independent methods yielding similar distance estimates to WX Pyx suggests that the inherent assumption in the Hertz estimate (i.e. the system has a disc) is valid. Thus it would appear that WX Pyx contains a partial disc around the white dwarf and it is mildly suggested that the mode of accretion is disc-fed. Further supporting evidence for the presence of the disc comes from the modulation at orbital period. The existence of such a modulation can be explained only by varying aspect of the bright spot formed at the location of stream-disc interaction which, again, requires the presence of the disc.

### 3.5 Constraints on the angle of inclination of the system

It is expected that CVs show an ellipsoidal variation in their near-IR light curves at the first harmonic of the orbital period. Such a variation would arise due to the aspect variation of the Roche-lobe filled distorted secondary star. Fixing the other known parameters of the system one can infer the angle of inclination *i* from the the shape of the phase curve. As seen in Fig. 1, the periodogram does not show significant power at the first harmonic of the orbital period shown as dashed line at the low frequency end of the spectrum. This suggests that the inclination angle of the binary system is low.

To estimate the upper limit of the inclination angle *i* we produced a binned phase curve at the first harmonic of the orbital period. This phase curve shows a maximum scatter of ±0.03 magnitudes. In order to estimate the upper limit of *i* we produced the synthetic phase curve using Wilson-Devinney light curve code (Wilson & Devinney 1971). Limb darkening values were obtained from interpolation of data in the table provided by Van Hamme (1993). The mass ratio *q* was varied between 0.2 and 0.6 and the appropriate inclination angle was obtained for each value of *q* such that the synthetic light curve shows a similar scatter as that observed in the data. We find that for any value of *q* in the chosen range, the inclination angle *i* is less then 30°. This is suggestive that the inclination angle of the system is small.

### 3.6 Mass transfer rate

The mass transfer rate $\dot{M}$ of the system can be estimated by comparing the accretion luminosity $L_{acc}$ and the released gravitational potential energy. When the mass is transferred from the inner

Lagrangian point to the white dwarf surface, the gravitational potential energy is released and radiates away, largely at X-ray wavelengths in the case of magnetic CVs.

To estimate the X-ray luminosity of WX Pyx we used the flux values given by Evans & Hellier (2007). These authors modeled the X-ray spectrum of WX Pyx using a combination of a non-thermal hard component and a thermal soft component. The unabsorbed bolometric X-ray flux corresponding to the soft and hard components are estimated to be $6.0 \times 10^{-13}$ ergs s$^{-1}$ cm$^{-2}$ and $7.51 \times 10^{-12}$ ergs s$^{-1}$ cm$^{-2}$ respectively giving a total X-ray flux of $8.11 \times 10^{-12}$ ergs s$^{-1}$ cm$^{-2}$. This flux is converted into the X-ray luminosity by the relation $L_x = 2\pi d^2 F_x$ where $L_x$ is the X-ray luminosity in ergs s$^{-1}$, $F_x$ is the X-ray bolometric flux in ergs s$^{-1}$ cm$^{-2}$ and $d$ is the distance. Here, the factor $2\pi$ is used instead of $4\pi$ to take into account that the X-ray emitting shock region is close to the white dwarf surface and half of the total emission is blocked by the stellar surface. Using a value of $d = 1.530$ kpc gives the X-ray luminosity $L_x = 1.1 \times 10^{33}$ ergs s$^{-1}$. Estimation of $L_{acc}$ is a complex process requiring information about various aspects including the IR to UV emission from the accreting material, absorption effect at UV and soft X-ray wavelengths and the contribution from X-rays above 10 keV (Warner 1995). However Warner (1995) indicates that $L_{acc}$ may be estimated, within an uncertainty of a factor of 2, by multiplying $L_x$ by 50. Therefore, $L_x$ was multiplied by this factor to estimate $L_{acc}$ which in turn is converted into the mass transfer rate $\dot{M}$ using $L_{acc} = GM_{WD}\dot{M}/R_{WD}$ where $L_{acc}$ is the total accretion luminosity and $M_{WD}$ and $R_{WD}$ are the mass and radius of the white dwarf respectively. $M_{WD}$ was chosen to lie in the range 1.31 to 1.4 $M_\odot$ as inferred by Evans & Hellier (2007) from modeling of the hard component of the X-ray data. $R_{WD}$ was calculated from the empirical mass radius relationship for white dwarfs given by Pringle & Webbink (1975). We obtain the mass transfer rate to lie in the range 0.6 to $1.0 \times 10^{17}$ g s$^{-1}$ or 0.95 to $1.6 \times 10^{-9} M_\odot$ yr$^{-1}$. This value of $\dot{M}$ is found to be fairly typical for IPs as has been compiled for several other such objects (Warner 1995).

### 3.7   Magnetic moment of the white dwarf

Assuming a magnetic white dwarf with spherically symmetric accretion, the magnetospheric radius $r_{mag}$ is defined to be the radius at which the magnetic pressure balances the ram pressure of the infalling material. Following the calculation given in Frank, King & Raine (2002) the magnetospheric radius is given by

$$r_{mag} = \left( \frac{2\pi^2 \mu^4}{\mu_0^2 GM_{WD}\dot{M}^2} \right)^{1/7} \tag{4}$$

where $\mu$ and $\mu_0$ are magnetic moment of white dwarf and permeability of free space respectively. However, if the white dwarf is accreting via a disc, the true magnetospheric radius $R_{mag}$ can be estimated from $R_{mag} = 0.5\, r_{mag}$.

If the white dwarf of the IP is in spin equilibrium it is assumed that the magnetospheric radius

$R_{mag}$ is very close to the co-rotation radius $R_{co}$ (e.g. Norton, Wynn & Somerscales 2004). Here $R_{co}$ is the radius at which the accreting material in local Keplerian motion co-rotates with the magnetic field of the white dwarf. Therefore,

$$R_{mag} \sim R_{co} = \left( \frac{GM_{WD}P_{spin}^2}{4\pi^2} \right)^{1/3} \tag{5}$$

Comparing equations (4) and (5), we get

$$\mu = 0.06 \left( G^{5/6} M_{WD}^{5/6} P_{spin}^{7/6} \dot{M}^{1/2} \right) \tag{6}$$

For WX Pyx, $\mu$ is thus estimated in the range 1.9 to $2.4 \times 10^{33}$ G cm$^3$ for a $M_{WD}$ value ranging between 1.31 and $1.4 M_\odot$. This result is consistent with the magnetic moments of several other IPs estimated by Warner (1995).

Norton et al. (2008) have simulated the accretion flow of magnetic CVs in a detailed study. They have shown that for a fixed orbital period and mass ratio, different regions in a diagnostic plot of the spin period versus magnetic moment, correspond to different geometries for the accretion viz. disc, stream, ring and propeller (Figs. 1 and 2 in Norton et al. 2008). For the orbital period and mass ratio specific for WX Pyx, we find that the estimated value of magnetic moment along with the spin period falls well inside the region corresponding to a disc type accretion. This also supports disc-fed accretion as the favored mode of accretion in WX Pyx.

## 4.  Summary

We have presented near infrared 1.25 $\mu$m *J* band photometry of WX Pyx covering a total duration of 22 hr spanning six nights from December, 2007 to February, 2010. Our motivation was to determine the spin period of the object from IR observations, an exercise which has not been done earlier, and if possible to also determine the orbital period. The frequency analysis of the light curve clearly indicates the presence of a spin period of 1559.2±0.2 sec for the white dwarf. However, the orbital period is less robustly determined. From the IR observations, a likely peak at 5.30±0.02 hr is seen in the power spectrum of the object which is argued to be the orbital period of the system. Subsequently, estimates are made of some of the physical properties and parameters of the system viz. the spectral type of the secondary star, the distance to the object, the mode of accretion, the angle of inclination of the system, the mass transfer rate and the magnetic moment of the white dwarf.

## 5.  Acknowledgments

# References

Bailey J., 1981, MNRAS, 197, 31

Bednarek W., Pabich J., 2011, MNRAS, 411, 1701

Beuermann K., Baraffe I., Kolb U., Weichhold M., 1998, A&A, 339, 518

Carpenter J.M., 2001, AJ, 121, 2851

Das R.K., Banerjee D.P.K., Ashok N.M., Chesneau O., 2008, MNRAS, 391, 1874

Evans P.A., Hellier C., 2007, ApJ, 663, 1277

Frank J., King A., Raine D.J., 2002, Accretion Power in Astrophysics Third ed., Cambridge
    University Press, Cambridge, p. 158

Hertz P., Grindlay J.E., 1984, ApJ, 278, 137

Hertz P., Bailyn C.D., Grindlay J.E., Garcia M.R., Cohn H., Lugger P.M., 1990, ApJ, 364, 251

Knigge C., 2006, MNRAS, 373, 484 (K2006)

Norton A.J., Wynn G.A., Somerscales R.V., 2004, ApJ, 672, 524

Norton A.J., Butters O.W., Parker T.L., Wynn G.A., 2008, ApJ, 672, 524

O'Donoghue D., 1996, MNRAS, 278, 1075

Patterson J., 1984, ApJS, 54, 443

Patterson J., 1994, PASP, 106, 209

Pringle J.E., Webbink R.F., 1975, MNRAS, 172, 493

Schlegel E.M., 2005, MNRAS, 433, 635

Van Hamme W., 1993, AJ, 106, 2096

Warner B., 1995, Cataclysmic Variable Stars, Cambridge Astrophys. Ser., Cambridge University
    Press, Cambridge, p. 397

Wilson R.E., Devinney E.J., 1971, ApJ, 166, 605

# Appendix

The appendix lists the *J* band photometric data of WX Pyx.

Table 3: *J* band photometric data of WX Pyx.

| Heliocentric JD | J | ΔJ | Heliocentric JD | J | ΔJ | Heliocentric JD | J | ΔJ |
|---|---|---|---|---|---|---|---|---|
| 2454452.3567 | 15.58 | 0.05 | 2454452.3821 | 15.47 | 0.06 | 2454452.4126 | 15.76 | 0.06 |
| 2454452.3592 | 15.56 | 0.05 | 2454452.3846 | 15.55 | 0.05 | 2454452.4151 | 15.62 | 0.05 |
| 2454452.3618 | 15.37 | 0.04 | 2454452.3897 | 15.59 | 0.05 | 2454452.4177 | 15.54 | 0.05 |
| 2454452.3643 | 15.39 | 0.05 | 2454452.3923 | 15.62 | 0.05 | 2454452.4202 | 15.43 | 0.05 |
| 2454452.3669 | 15.35 | 0.05 | 2454452.3948 | 15.75 | 0.05 | 2454452.4227 | 15.46 | 0.05 |
| 2454452.3694 | 15.37 | 0.05 | 2454452.3973 | 15.59 | 0.05 | 2454452.4253 | 15.56 | 0.05 |
| 2454452.3719 | 15.47 | 0.06 | 2454452.4024 | 15.48 | 0.05 | 2454452.4278 | 15.73 | 0.05 |
| 2454452.3745 | 15.53 | 0.05 | 2454452.4050 | 15.45 | 0.05 | 2454452.4303 | 15.86 | 0.05 |
| 2454452.3770 | 15.54 | 0.05 | 2454452.4075 | 15.48 | 0.05 | 2454452.4329 | 15.70 | 0.05 |
| 2454452.3796 | 15.53 | 0.05 | 2454452.4100 | 15.65 | 0.05 | 2454452.4380 | 15.62 | 0.05 |

| Heliocentric JD | $J$ | $\Delta J$ | Heliocentric JD | $J$ | $\Delta J$ | Heliocentric JD | $J$ | $\Delta J$ |
|---|---|---|---|---|---|---|---|---|
| 2454452.4405 | 15.58 | 0.05 | 2454453.3119 | 15.64 | 0.04 | 2454453.4028 | 15.66 | 0.04 |
| 2454452.4430 | 15.61 | 0.05 | 2454453.3140 | 15.75 | 0.04 | 2454453.4049 | 15.68 | 0.05 |
| 2454452.4456 | 15.75 | 0.06 | 2454453.3161 | 15.61 | 0.05 | 2454453.4070 | 15.64 | 0.04 |
| 2454452.4481 | 15.80 | 0.06 | 2454453.3183 | 15.42 | 0.04 | 2454453.4091 | 15.54 | 0.04 |
| 2454452.4507 | 15.57 | 0.05 | 2454453.3204 | 15.31 | 0.05 | 2454453.4112 | 15.45 | 0.04 |
| 2454452.4532 | 15.43 | 0.05 | 2454453.3225 | 15.42 | 0.04 | 2454453.4133 | 15.36 | 0.05 |
| 2454452.4557 | 15.51 | 0.06 | 2454453.3246 | 15.41 | 0.05 | 2454453.4154 | 15.45 | 0.04 |
| 2454452.4583 | 15.42 | 0.05 | 2454453.3267 | 15.41 | 0.04 | 2454453.4175 | 15.47 | 0.04 |
| 2454452.4608 | 15.38 | 0.05 | 2454453.3288 | 15.70 | 0.05 | 2454453.4196 | 15.62 | 0.04 |
| 2454452.4659 | 15.81 | 0.05 | 2454453.3309 | 15.74 | 0.04 | 2454453.4217 | 15.64 | 0.04 |
| 2454452.4684 | 15.54 | 0.05 | 2454453.3330 | 15.84 | 0.05 | 2454453.4238 | 15.65 | 0.04 |
| 2454452.4710 | 15.48 | 0.06 | 2454453.3351 | 15.68 | 0.04 | 2454453.4259 | 15.50 | 0.05 |
| 2454452.4735 | 15.52 | 0.05 | 2454453.3372 | 15.51 | 0.04 | 2454453.4302 | 15.42 | 0.05 |
| 2454452.4761 | 15.34 | 0.05 | 2454453.3393 | 15.40 | 0.04 | 2454453.4323 | 15.29 | 0.04 |
| 2454452.4786 | 15.37 | 0.06 | 2454453.3414 | 15.42 | 0.04 | 2454453.4344 | 15.31 | 0.04 |
| 2454452.4811 | 15.52 | 0.05 | 2454453.3435 | 15.45 | 0.04 | 2454453.4365 | 15.40 | 0.04 |
| 2454452.4837 | 15.73 | 0.05 | 2454453.3456 | 15.48 | 0.05 | 2454453.4386 | 15.55 | 0.05 |
| 2454452.4862 | 15.58 | 0.05 | 2454453.3477 | 15.64 | 0.04 | 2454453.4407 | 15.62 | 0.04 |
| 2454452.4888 | 15.45 | 0.05 | 2454453.3499 | 15.73 | 0.05 | 2454453.4428 | 15.59 | 0.04 |
| 2454452.4913 | 15.47 | 0.05 | 2454453.3543 | 15.61 | 0.04 | 2454453.4449 | 15.48 | 0.05 |
| 2454452.4938 | 15.38 | 0.05 | 2454453.3564 | 15.41 | 0.05 | 2454453.4470 | 15.42 | 0.04 |
| 2454452.4964 | 15.43 | 0.05 | 2454453.3585 | 15.36 | 0.04 | 2454453.4491 | 15.30 | 0.05 |
| 2454452.4989 | 15.62 | 0.05 | 2454453.3606 | 15.46 | 0.04 | 2454453.4512 | 15.29 | 0.04 |
| 2454452.5015 | 15.66 | 0.05 | 2454453.3627 | 15.50 | 0.05 | 2454453.4533 | 15.31 | 0.04 |
| 2454452.5040 | 15.72 | 0.05 | 2454453.3649 | 15.60 | 0.04 | 2454453.4554 | 15.41 | 0.04 |
| 2454452.5065 | 15.53 | 0.06 | 2454453.3670 | 15.69 | 0.04 | 2454453.4575 | 15.51 | 0.05 |
| 2454452.5091 | 15.49 | 0.05 | 2454453.3691 | 15.77 | 0.04 | 2454453.4597 | 15.49 | 0.04 |
| 2454452.5116 | 15.48 | 0.05 | 2454453.3712 | 15.63 | 0.05 | 2454453.4618 | 15.38 | 0.05 |
| 2454452.5141 | 15.44 | 0.05 | 2454453.3733 | 15.61 | 0.04 | 2454453.4639 | 15.34 | 0.05 |
| 2454452.5167 | 15.58 | 0.05 | 2454453.3754 | 15.38 | 0.04 | 2454453.4660 | 15.36 | 0.05 |
| 2454452.5192 | 15.65 | 0.05 | 2454453.3775 | 15.39 | 0.05 | 2454483.2813 | 15.45 | 0.06 |
| 2454452.5218 | 15.80 | 0.05 | 2454453.3796 | 15.37 | 0.05 | 2454483.2835 | 15.42 | 0.06 |
| 2454452.5243 | 15.44 | 0.05 | 2454453.3817 | 15.48 | 0.04 | 2454483.2858 | 15.58 | 0.06 |
| 2454452.5268 | 15.44 | 0.05 | 2454453.3838 | 15.68 | 0.05 | 2454483.2880 | 15.56 | 0.06 |
| 2454452.5294 | 15.30 | 0.06 | 2454453.3859 | 15.71 | 0.05 | 2454483.2925 | 15.49 | 0.06 |
| 2454452.5319 | 15.25 | 0.05 | 2454453.3880 | 15.59 | 0.05 | 2454483.2948 | 15.54 | 0.06 |
| 2454452.5345 | 15.45 | 0.05 | 2454453.3901 | 15.58 | 0.04 | 2454483.2970 | 15.40 | 0.06 |
| 2454452.5370 | 15.70 | 0.05 | 2454453.3943 | 15.40 | 0.04 | 2454483.2993 | 15.42 | 0.06 |
| 2454452.5395 | 15.67 | 0.06 | 2454453.3965 | 15.33 | 0.04 | 2454483.3015 | 15.50 | 0.06 |
| 2454453.3077 | 15.31 | 0.04 | 2454453.3986 | 15.29 | 0.05 | 2454483.3038 | 15.45 | 0.06 |
| 2454453.3098 | 15.52 | 0.04 | 2454453.4007 | 15.48 | 0.05 | 2454483.3060 | 15.65 | 0.05 |

| Heliocentric JD | $J$ | $\Delta J$ | Heliocentric JD | $J$ | $\Delta J$ | Heliocentric JD | $J$ | $\Delta J$ |
|---|---|---|---|---|---|---|---|---|
| 2454483.3083 | 15.67 | 0.06 | 2454483.4028 | 15.58 | 0.06 | 2454909.2036 | 15.61 | 0.06 |
| 2454483.3105 | 15.48 | 0.06 | 2454483.4051 | 15.53 | 0.06 | 2454909.2058 | 15.70 | 0.05 |
| 2454483.3128 | 15.42 | 0.06 | 2454483.4073 | 15.33 | 0.07 | 2454909.2081 | 15.63 | 0.06 |
| 2454483.3150 | 15.42 | 0.06 | 2454483.4096 | 15.47 | 0.06 | 2454909.2103 | 15.72 | 0.06 |
| 2454483.3173 | 15.41 | 0.06 | 2454483.4118 | 15.55 | 0.06 | 2454909.2126 | 15.48 | 0.05 |
| 2454483.3195 | 15.51 | 0.06 | 2454909.1134 | 15.48 | 0.06 | 2454909.2171 | 15.36 | 0.05 |
| 2454483.3218 | 15.59 | 0.06 | 2454909.1156 | 15.59 | 0.06 | 2454909.2193 | 15.46 | 0.06 |
| 2454483.3240 | 15.64 | 0.06 | 2454909.1179 | 15.59 | 0.06 | 2454909.2238 | 15.63 | 0.06 |
| 2454483.3263 | 15.78 | 0.06 | 2454909.1201 | 15.62 | 0.06 | 2454909.2261 | 15.81 | 0.05 |
| 2454483.3285 | 15.67 | 0.06 | 2454909.1224 | 15.60 | 0.06 | 2454909.2283 | 15.74 | 0.06 |
| 2454483.3308 | 15.51 | 0.06 | 2454909.1246 | 15.54 | 0.06 | 2454909.2306 | 15.64 | 0.06 |
| 2454483.3330 | 15.46 | 0.06 | 2454909.1269 | 15.46 | 0.06 | 2454909.2328 | 15.49 | 0.05 |
| 2454483.3353 | 15.55 | 0.05 | 2454909.1291 | 15.40 | 0.06 | 2454909.2351 | 15.37 | 0.06 |
| 2454483.3375 | 15.60 | 0.06 | 2454909.1314 | 15.54 | 0.06 | 2454909.2373 | 15.36 | 0.06 |
| 2454483.3398 | 15.52 | 0.06 | 2454909.1336 | 15.60 | 0.06 | 2454909.2396 | 15.50 | 0.06 |
| 2454483.3421 | 15.71 | 0.07 | 2454909.1359 | 15.72 | 0.05 | 2454909.2418 | 15.69 | 0.06 |
| 2454483.3443 | 15.79 | 0.06 | 2454909.1381 | 15.72 | 0.06 | 2454909.2441 | 15.67 | 0.05 |
| 2454483.3466 | 15.69 | 0.07 | 2454909.1404 | 15.64 | 0.06 | 2454909.2463 | 15.62 | 0.06 |
| 2454483.3488 | 15.47 | 0.06 | 2454909.1426 | 15.49 | 0.06 | 2454909.2531 | 15.37 | 0.06 |
| 2454483.3511 | 15.35 | 0.06 | 2454909.1449 | 15.60 | 0.06 | 2454909.2553 | 15.37 | 0.06 |
| 2454483.3533 | 15.46 | 0.06 | 2454909.1471 | 15.55 | 0.06 | 2454909.2576 | 15.48 | 0.06 |
| 2454483.3556 | 15.48 | 0.07 | 2454909.1494 | 15.59 | 0.06 | 2454909.2598 | 15.68 | 0.05 |
| 2454483.3578 | 15.51 | 0.06 | 2454909.1516 | 15.53 | 0.06 | 2454909.2621 | 15.61 | 0.06 |
| 2454483.3601 | 15.61 | 0.06 | 2454909.1539 | 15.68 | 0.06 | 2454909.2666 | 15.50 | 0.06 |
| 2454483.3623 | 15.54 | 0.06 | 2454909.1561 | 15.58 | 0.06 | 2454909.2688 | 15.56 | 0.06 |
| 2454483.3646 | 15.58 | 0.05 | 2454909.1606 | 15.40 | 0.06 | 2454909.2711 | 15.54 | 0.06 |
| 2454483.3668 | 15.56 | 0.06 | 2454909.1629 | 15.47 | 0.07 | 2454909.2733 | 15.50 | 0.07 |
| 2454483.3691 | 15.43 | 0.06 | 2454909.1651 | 15.52 | 0.06 | 2454909.2756 | 15.53 | 0.05 |
| 2454483.3713 | 15.39 | 0.06 | 2454909.1674 | 15.53 | 0.06 | 2454909.2778 | 15.59 | 0.05 |
| 2454483.3736 | 15.44 | 0.07 | 2454909.1696 | 15.72 | 0.06 | 2454910.0994 | 15.37 | 0.06 |
| 2454483.3758 | 15.70 | 0.06 | 2454909.1719 | 15.83 | 0.06 | 2454910.1015 | 15.38 | 0.05 |
| 2454483.3781 | 15.64 | 0.06 | 2454909.1764 | 15.59 | 0.06 | 2454910.1058 | 15.33 | 0.05 |
| 2454483.3803 | 15.53 | 0.06 | 2454909.1786 | 15.56 | 0.06 | 2454910.1079 | 15.44 | 0.05 |
| 2454483.3826 | 15.54 | 0.06 | 2454909.1809 | 15.52 | 0.05 | 2454910.1100 | 15.71 | 0.06 |
| 2454483.3848 | 15.45 | 0.07 | 2454909.1831 | 15.47 | 0.06 | 2454910.1143 | 15.42 | 0.05 |
| 2454483.3893 | 15.47 | 0.06 | 2454909.1876 | 15.61 | 0.06 | 2454910.1164 | 15.44 | 0.05 |
| 2454483.3916 | 15.42 | 0.07 | 2454909.1899 | 15.66 | 0.06 | 2454910.1207 | 15.36 | 0.06 |
| 2454483.3938 | 15.55 | 0.06 | 2454909.1921 | 15.78 | 0.05 | 2454910.1228 | 15.39 | 0.05 |
| 2454483.3961 | 15.77 | 0.06 | 2454909.1944 | 15.51 | 0.06 | 2454910.1249 | 15.52 | 0.05 |
| 2454483.3983 | 15.59 | 0.06 | 2454909.1966 | 15.57 | 0.05 | 2454910.1271 | 15.59 | 0.05 |
| 2454483.4006 | 15.59 | 0.06 | 2454909.2013 | 15.48 | 0.06 | 2454910.1292 | 15.75 | 0.06 |

| Heliocentric JD | $J$ | $\Delta J$ | Heliocentric JD | $J$ | $\Delta J$ | Heliocentric JD | $J$ | $\Delta J$ |
|---|---|---|---|---|---|---|---|---|
| 2454910.1313 | 15.47 | 0.05 | 2454910.2144 | 15.38 | 0.05 | 2455250.2234 | 15.62 | 0.07 |
| 2454910.1334 | 15.52 | 0.05 | 2454910.2165 | 15.43 | 0.06 | 2455250.2255 | 15.48 | 0.07 |
| 2454910.1356 | 15.46 | 0.05 | 2454910.2186 | 15.67 | 0.06 | 2455250.2276 | 15.57 | 0.08 |
| 2454910.1377 | 15.44 | 0.05 | 2454910.2208 | 15.59 | 0.06 | 2455250.2297 | 15.54 | 0.07 |
| 2454910.1398 | 15.41 | 0.05 | 2454910.2229 | 15.64 | 0.06 | 2455250.2318 | 15.47 | 0.07 |
| 2454910.1420 | 15.40 | 0.06 | 2454910.2250 | 15.51 | 0.05 | 2455250.2339 | 15.69 | 0.07 |
| 2454910.1441 | 15.72 | 0.06 | 2454910.2272 | 15.49 | 0.06 | 2455250.2360 | 15.66 | 0.07 |
| 2454910.1462 | 15.64 | 0.06 | 2454910.2293 | 15.41 | 0.06 | 2455250.2381 | 15.80 | 0.07 |
| 2454910.1484 | 15.58 | 0.05 | 2454910.2314 | 15.45 | 0.05 | 2455250.2402 | 15.68 | 0.07 |
| 2454910.1526 | 15.52 | 0.06 | 2454910.2335 | 15.62 | 0.06 | 2455250.2423 | 15.58 | 0.07 |
| 2454910.1547 | 15.39 | 0.05 | 2454910.2357 | 15.58 | 0.05 | 2455250.2444 | 15.36 | 0.07 |
| 2454910.1569 | 15.42 | 0.05 | 2454910.2378 | 15.67 | 0.06 | 2455250.2465 | 15.38 | 0.07 |
| 2454910.1590 | 15.43 | 0.05 | 2454910.2399 | 15.69 | 0.06 | 2455250.2486 | 15.53 | 0.06 |
| 2454910.1611 | 15.58 | 0.06 | 2454910.2421 | 15.46 | 0.05 | 2455250.2507 | 15.52 | 0.06 |
| 2454910.1633 | 15.59 | 0.06 | 2454910.2485 | 15.41 | 0.05 | 2455250.2528 | 15.68 | 0.07 |
| 2454910.1654 | 15.63 | 0.05 | 2454910.2527 | 15.71 | 0.06 | 2455250.2549 | 15.66 | 0.07 |
| 2454910.1675 | 15.53 | 0.05 | 2454910.2548 | 15.78 | 0.05 | 2455250.2570 | 15.60 | 0.07 |
| 2454910.1696 | 15.49 | 0.05 | 2454910.2570 | 15.61 | 0.06 | 2455250.2591 | 15.63 | 0.07 |
| 2454910.1739 | 15.34 | 0.05 | 2454910.2591 | 15.49 | 0.05 | 2455250.2612 | 15.35 | 0.08 |
| 2454910.1760 | 15.36 | 0.06 | 2455250.1981 | 15.73 | 0.08 | 2455250.2633 | 15.43 | 0.07 |
| 2454910.1782 | 15.34 | 0.05 | 2455250.2003 | 15.63 | 0.07 | 2455250.2654 | 15.58 | 0.06 |
| 2454910.1803 | 15.51 | 0.05 | 2455250.2024 | 15.68 | 0.07 | 2455250.2675 | 15.63 | 0.07 |
| 2454910.1824 | 15.58 | 0.06 | 2455250.2045 | 15.50 | 0.08 | 2455250.2696 | 15.48 | 0.07 |
| 2454910.1888 | 15.44 | 0.06 | 2455250.2066 | 15.43 | 0.07 | 2455250.2717 | 15.58 | 0.07 |
| 2454910.1909 | 15.35 | 0.05 | 2455250.2087 | 15.32 | 0.07 | 2455250.2738 | 15.74 | 0.08 |
| 2454910.1931 | 15.37 | 0.06 | 2455250.2108 | 15.60 | 0.07 | 2455250.2759 | 15.52 | 0.07 |
| 2454910.1952 | 15.45 | 0.05 | 2455250.2129 | 15.46 | 0.07 | 2455250.2780 | 15.60 | 0.08 |
| 2454910.1973 | 15.56 | 0.06 | 2455250.2150 | 15.44 | 0.07 | 2455250.2801 | 15.41 | 0.08 |
| 2454910.1995 | 15.51 | 0.06 | 2455250.2171 | 15.70 | 0.07 | 2455250.2822 | 15.42 | 0.07 |
| 2454910.2037 | 15.57 | 0.06 | 2455250.2192 | 15.66 | 0.07 | 2455250.2843 | 15.59 | 0.07 |
| 2454910.2059 | 15.46 | 0.06 | 2455250.2213 | 15.55 | 0.07 | 2455250.2885 | 15.68 | 0.07 |